

Geometry-Induced Spin Filtering in Photoemission Maps from WTe_2 Surface States

Tristan Heider¹,^{*} Gustav Bihlmayer², Jakub Schusser^{3,4}, Friedrich Reinert⁴, Jan Minár³,
Stefan Blügel², Claus M. Schneider^{1,5,6}, and Lukasz Plucinski^{1,*}

¹*Peter Grünberg Institut (PGI-6), Forschungszentrum Jülich GmbH, 52428 Jülich, Germany*


²*Peter Grünberg Institut (PGI-1) and Institute for Advanced Simulation (IAS-1),
Forschungszentrum Jülich and JARA, 52428 Jülich, Germany*

³*New Technologies-Research Center, University of West Bohemia, 30614 Pilsen, Czech Republic*

⁴*Experimentelle Physik VII and Würzburg-Dresden Cluster of Excellence ct.qmat,
Universität Würzburg, 97070 Würzburg, Germany*

⁵*Fakultät für Physik, Universität Duisburg-Essen, 47048 Duisburg, Germany*

⁶*Physics Department, University of California, Davis, California 95616, USA*

 (Received 14 April 2022; revised 22 August 2022; accepted 24 February 2023; published 5 April 2023)

We demonstrate that an important quantum material WTe_2 exhibits a new type of geometry-induced spin filtering effect in photoemission, stemming from low symmetry that is responsible for its exotic transport properties. Through the laser-driven spin-polarized angle-resolved photoemission Fermi surface mapping, we showcase highly asymmetric spin textures of electrons photoemitted from the surface states of WTe_2 . Such asymmetries are not present in the initial state spin textures, which are bound by the time-reversal and crystal lattice mirror plane symmetries. The findings are reproduced qualitatively by theoretical modeling within the one-step model photoemission formalism. The effect could be understood within the free-electron final state model as an interference due to emission from different atomic sites. The observed effect is a manifestation of time-reversal symmetry breaking of the initial state in the photoemission process, and as such it cannot be eliminated, but only its magnitude influenced, by special experimental geometries.

DOI: [10.1103/PhysRevLett.130.146401](https://doi.org/10.1103/PhysRevLett.130.146401)

Introduction.— WTe_2 is a semimetallic two-dimensional (2D) quantum material that exhibits a nonsaturating magnetoresistance up to 60 T [1]. It has been debated whether the bulk electron and hole pockets in WTe_2 slightly overlap leading to the Weyl type-II topological phase [2,3], with a conjecture that the surface electronic structure would be virtually indistinguishable for topological and trivial phases [4]. When thinned down to a monolayer, WTe_2 enables the realization of high-temperature quantum Hall phases [5] and gate-controlled superconductivity [6,7]. In nonmagnetic systems, the first-order Hall response vanishes at zero magnetic field due to symmetry arguments. However, the second-order correction leads to the recently discovered [8–11] nonlinear Hall effect (NLHE) in systems of reduced symmetry. Few-layer WTe_2 has been the first system in which the NLHE has been demonstrated [9,10] due to the presence of a single mirror plane and a related existence of polar axes both in and out of plane of the layers.

Early high-resolution angle-resolved photoemission (ARPES) on WTe_2 [12,13] focused on imaging bulk electron and hole pockets with the motivation to explain the nonsaturating magnetoresistance. The prediction of possible type-II Weyl states in WTe_2 [2] has stimulated further research on its electronic structure. Subsequent ARPES studies focused on details of the surface electronic

structure on polar surfaces [4], their temperature dependence [14], influence of correlation effects [15], and effects of deposition of alkali submonolayers [16]. A more complete understanding of the electronic properties of WTe_2 requires detailed characterization of not only energetic positions of the bands, but also their spin character with its relation to the crystal symmetries.

Using the newly developed high-resolution laser-driven spin-polarized ARPES (SARPES) spectrometer, we demonstrate for the first time the spin texture of the Fermi level photoemission map measured with 6 eV photons. Previous SARPES studies only probed selected regions in the Brillouin zone (BZ) [17–19]. We further demonstrate that the symmetry of the ARPES spin texture reflects the WTe_2 surface symmetry with a single mirror plane present and not the initial state spin symmetry. Therefore, we directly demonstrate that the ARPES photocurrent carries additional information beyond the initial band structure spin texture, due to what we call the “geometry-induced spin filtering effect.”

The results are analyzed by comparison to density functional theory (DFT) calculations. The results obtained in the linearized augmented plane wave (LAPW) scheme show that the initial state spin texture follows the expected axial vector transformation rules of a single mirror plane and time reversal. Further one-step model photoemission

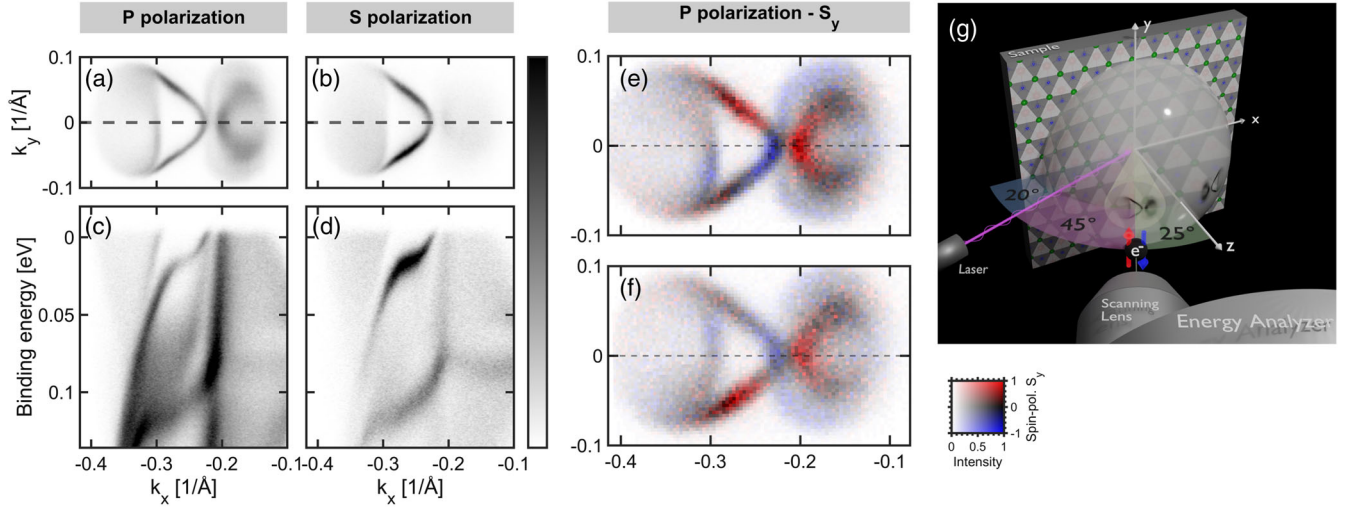


FIG. 1. (a),(b) Spin-integrated laser ARPES Fermi surface maps measured with p - and s -polarized light. (c),(d) Corresponding energy dispersions $E(k_x)$ for $k_y = 0$ as indicated by the dashed lines in (a) and (b). (e),(f) Experimental laser-SARPES 57×89 pixel Fermi surface maps taken at two nearby spots on the same cleave. The false color scale refers to the spin polarization S_{fy} in the ensemble of the photoemitted electrons. (g) Schematic geometry of the SARPES experiment. The maps were measured using the lens deflector system collecting the emission angles indicated by the yellow cone with the sample rotated by $\theta = 25^\circ$ with respect to the lens axis using p -polarized light and probing the spin along the y axis, as defined in (g).

calculations within the Korringa-Kohn-Rostoker (KKR) scheme reproduce the (broken) symmetry properties of the experimental data. Finally, within the free-electron final state ARPES model, we identify the origin of the observed asymmetries as an interference of the emission from different atomic sites.

Methods.—The sample (Td-WTe₂ single crystal, space group $Pmn2_1$, purchased from HQ Graphene) was glued to the molybdenum sample plate by a silver epoxy. We used p - or s -polarized light from the LEOS Solutions continuous wave laser with $h\nu = 6.02$ eV focused down to ~ 50 μm , the MB Scientific A1 hemispherical electron analyzer, and the exchange-scattering Focus GmbH FERRUM spin detector [20]. Spectrometers based on a similar design are in operation at synchrotron light sources [21,22]. The mirror plane of WTe₂ was aligned parallel to the entrance slit of the A1 spectrometer. The mechanoelectrostatic lens deflector system of A1 allows mapping of the emission angle over approximately $\pm 15^\circ$ in both k_x and k_y directions, therefore allowing for point-by-point k_x vs k_y mapping in the spin-polarized mode without rotating the sample. All measurements were carried out at ~ 15 K at the pressure in the analyzer chamber $< 5 \times 10^{-11}$ mbar.

The initial state band structure was calculated using DFT in the generalized gradient approximation [23]. We use the full-potential LAPW method in film geometry as implemented in the FLEUR code [24]. Photoemission calculations were performed within the one-step model formalism as implemented in the fully relativistic KKR method [18,25].

Further details on methods are provided in Sec. SI of the Supplemental Material [26].

Results.—Figures 1(a)–1(d) show the high-resolution ARPES maps measured with the 6 eV laser, which are in quantitative agreement with previously published results [4,14]. Figures 1(e) and 1(f) show the spin-polarized Fermi surface maps with p -polarized light from two different spots on the sample in the off-normal geometry described in Fig. 1(g), using the A1 lens deflector system to map the important portion of the BZ without rotating the sample. The use of the deflector system is critical to ensure that the entire map is taken with the laser beam focused on precisely the same spot on the sample. Both maps show the familiar shape previously reported in Refs. [4,14]; however, their spin textures are different and highly asymmetric. Supplemental Material Fig. S4 [26] shows SARPES spin texture taken with s -polarized light, where the spin polarization, albeit smaller, is also observed.

The crystal lattice of WTe₂ is shown schematically in Figs. 2(a) and 2(b). The surface of WTe₂ exhibits a single \mathcal{M}_x mirror plane, while the y and z directions are polar (see Sec. SII of the Supplemental Material [26] and Ref. [33]). By convention, the polarity along the z axis has been defined as surface A (or top) and B (or bottom), as depicted in Fig. 2(a), with radically different Fermi contours measured on these surfaces [4,16]. The shapes of Fermi surfaces from Figs. 1(a), 1(b), 1(e), and 1(f) have been associated with the surface B .

The glide-reflection operation $(1/2 + x, -y, 1/2 + z)$ of the $Pmn2_1$ space group [33] shows that adjacent terraces, which we call $D1$ and $D2$, have reversed polarity along y , as shown explicitly in Fig. 2(b). Cleaved transition-metal dichalcogenides typically exhibit macroscopically large

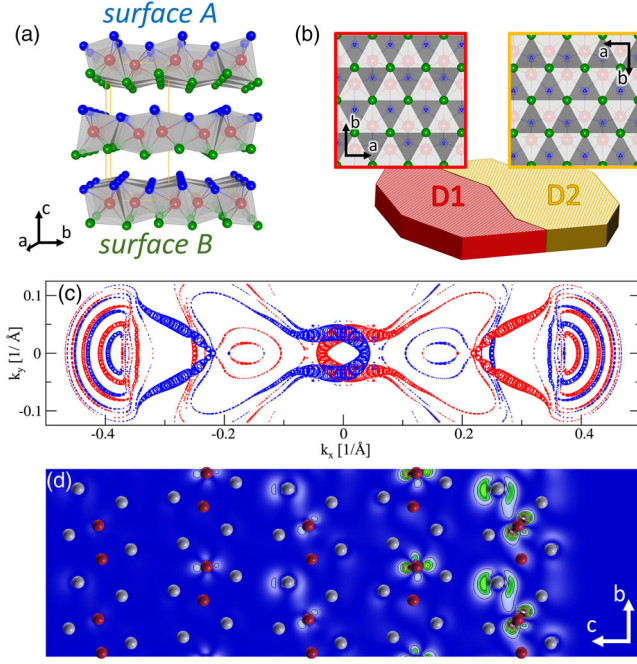


FIG. 2. Crystal geometry and initial state spin textures. (a) The 3D impression of the WTe₂ crystal structure. (b) The probed surface with two possible terminations, which we label D1 and D2. (c) The S_y component of the theoretical Fermi level spin texture, which is the same for both domains. The size of the symbols corresponds to the spin polarization in the first layer (containing two formula units). (d) The surface state charge density in real space at $k_x = -0.3 \text{ \AA}^{-1}$ and initial energy -25 meV (see Supplemental Material Fig. S6 [26]).

terraces of the sizes of $100 \text{ }\mu\text{m}$ or larger, and with our laser beam spot of $50 \text{ }\mu\text{m}$ we can routinely address a single terrace; therefore, we assume that the spectra in Figs. 1(e) and 1(f) are taken on single terraces of reversed polarity.

Since WTe₂ is nonmagnetic, the spin expectation value S_i of the initial state has to follow $S_i(\mathbf{k}_i) = -S_i(-\mathbf{k}_i)$. For the surface states, by combining this with the axial vector rules for the \mathcal{M}_x mirror plane, one gets $S_{iy}(k_{ix}, k_{iy}) = S_{iy}(k_{ix}, -k_{iy})$, and our theoretical initial state spin texture for surface B shown in Fig. 2(c) obeys this symmetry. However, this symmetry is broken in Figs. 1(e) and 1(f). Already, from the visual inspection in some portions of these SARPES maps, S_{fy} changes sign between (k_{fx}, k_{fy}) and $(k_{fx}, -k_{fy})$, while in other portions it does not. Here, \mathbf{k}_f refers to the momentum and S_{fy} to the y component of the spin expectation value in the ensemble of photoemitted electrons measured by SARPES. We note that, in ARPES, the component of \mathbf{k}_f parallel to the surface is related to the off-normal emission angle θ and kinetic energy E_{kin} by $k_{f\parallel} = (1/\hbar)\sqrt{2mE_{\text{kin}}}\sin\theta$ and the parallel momentum component is conserved in the photoemission process, i.e., $\mathbf{k}_{f\parallel} = \mathbf{k}_{i\parallel}$.

A visual inspection suggests that Fig. 1(e) can be transformed into Fig. 1(f) by $S_{fy}(k_{fx}, k_{fy}) \rightarrow S_{fy}(k_{fx}, -k_{fy})$, which is indeed confirmed by a quantitative standard deviation analysis, see Sec. SI of the Supplemental Material [26]. This can be explained by the symmetry operation $(1/2 + x, -y, 1/2 + z)$ of the $Pmn2_1$ space group, assuming Figs. 1(e) and 1(f) are measured on adjacent terraces. Here the $1/2 + z$ operation indicates switching into the adjacent layer or rather terrace. Reciprocal methods such as ARPES are insensitive to lateral shifts of the entire lattice and therefore the $1/2$ component in the $1/2 + x$ operation can be ignored when considering the symmetries of ARPES. This means that SARPES maps from adjacent terraces are connected by the \mathcal{M}_y mirror operation. Since in our geometry neither the s - nor the p -polarized light is breaking the \mathcal{M}_y mirror plane, this leads to $\mathcal{M}_y\{S_{fy}^{D1}(k_{fx}, k_{fy})\} = S_{fy}^{D2}(k_{fx}, -k_{fy})$ for our ARPES maps from adjacent terraces D1 and D2 [Fig. 2(b)].

Figure 2(d) shows that the surface state on surface B is primarily localized within the first two WTe₂ monolayers. One can also recognize a complex orbital structure of the surface state, with different orbital orientations contributing within the first and the second WTe₂ layers indicating radical breaking of the \mathcal{M}_y mirror symmetry. Approximate shapes of p_z orbitals on Te atoms and d_{z^2} on W atoms can be recognized; however, they are not perfectly aligned along the z axis.

Figures 3(a)–3(h) present one-step model calculations of the spin polarization from WTe₂ at our experimental parameters and at the theoretical KKR binding energy $E_B = 0.15 \text{ eV}$ that best matches the experimental Fermi level (see Sec. SIII of the Supplemental Material [26] for details). For both the p - and s -polarized light and for both the free-electron final state (FEFS) and time-reversed (TR)-LEED final states, the S_{fy} ARPES spin textures exhibit broken \mathcal{M}_y symmetry, unlike in the initial state map in Fig. 2(c), but in qualitative agreement with the experiment. Considering the system of a sample together with an incident light, for s -polarized light the \mathcal{M}_x symmetry of the WTe₂ is conserved, because in this case the \mathbf{E} field of the light is along the y axis, leading to $S_{fy}(k_{fx}, k_{fy}) = -S_{fy}(-k_{fx}, k_{fy})$. For the p -polarized light, \mathcal{M}_x is broken due to \mathbf{E} being within the xz plane.

Figures 3(i)–3(m) theoretically explore the parameter space for p - and s -polarized light. While the asymmetry effect is confirmed, for both polarizations it strongly depends on photon and binding energies. In contrast to the experiment, at the experimental parameters its magnitude is predicted to be smaller for p -polarized light than for s -polarized light. Comparison between Figs. 3(i) and 3(j) reveals the influence of FEFS and TR-LEED final states on the predicted polarization. In particular, for s -polarized light the difference for the point S3 leads to change of the sign of spin polarization, stressing the importance of final states in quantitative analysis.

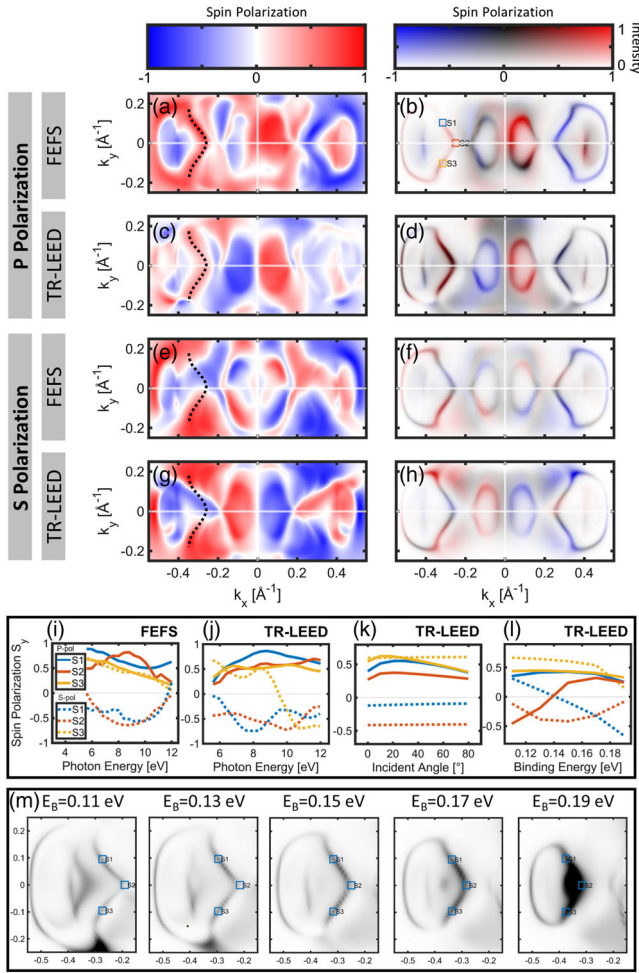


FIG. 3. One-step model calculation of spin polarization S_y (a)–(d) p -polarized and (e)–(h) s -polarized light. (a),(c),(e),(g) Pure spin polarization. (b),(d),(f),(h) Weighted by photoemission intensity. (a),(b),(e),(f) FEFS was used. (c),(d),(g),(h) The TR-LEED final state was used. (i)–(k) The magnitude of S_y at 3-momenta S1–S3 indicated in (b); solid lines are for p -polarized light and dashed lines are for s -polarized light. (i),(j) The dependence on photon energy for the FEFS and TR-LEED final states, respectively. (k) The dependence on the off-normal light incidence angle. (l) The dependence on binding energy for the momenta indicated in (m), where TR-LEED maps (with p -polarized light) at several binding energies are shown. For convenience, the dashed lines in (a), (c), (e), and (g) indicate the location of the surface state.

Dashed lines in Fig. 3(k) show very weak dependence of the spin polarization on the light incident angle θ_{ph} , as expected for the s -polarized light. Since they refer to the constant parallel momenta S1–S3, the remaining dependence is related to small, but in this case non-negligible, shifts induced by the parallel component of the photon momentum $k_{ph\parallel} \simeq 0.003 \text{ \AA}^{-1} \sin \theta_{ph}$.

The origin of the spin filtering effect can be understood within the tight-binding (TB) formalism taking into

account the FEFS matrix element $w(k_{fx}, k_{fy}, k_{fz}) = \langle e^{i\mathbf{k}_f \cdot \mathbf{r}} | \psi_i(k_{ix}, k_{iy}, \mathbf{r}) \rangle$ [34,35], where ψ_i is the initial surface state eigenfunction with an eigenvalue (binding energy) E_B . Assuming a system of N orbitals $|j\rangle$ at positions \mathbf{r}_j , we can write $\psi_i(k_{ix}, k_{iy}, \mathbf{r}) = \sum_{j=1}^N C_j |j\rangle \delta(\mathbf{r} - \mathbf{r}_j)$. The FEFS matrix element is essentially a Fourier transform and therefore different sites \mathbf{r}_j will lead to phase shifts $e^{i\mathbf{k}_f \cdot \mathbf{r}_j}$. Since within the TB formalism only discrete sites \mathbf{r}_j are considered, the matrix element will have a form of a sum $w(k_{fx}, k_{fy}, k_{fz}) = \sum_{j=1}^N e^{i\mathbf{k}_f \cdot \mathbf{r}_j} C_j |j\rangle$.

Relating to squares S1 and S3 in Fig. 3(b), for a periodic system, probing initial parallel momenta $\mathbf{k}_{iS1} = (k_{ix}, k_{iy})$ and $\mathbf{k}_{iS3} = (k_{ix}, -k_{iy})$ by ARPES requires measuring electrons emitted along $\mathbf{k}_{fS1} = (k_{ix}, k_{iy}, k_{fz})$ and $\mathbf{k}_{fS3} = (k_{ix}, -k_{iy}, k_{fz})$. For a particular photon energy $h\nu$, k_{fz} can be determined through $|\mathbf{k}_f| = (1/\hbar)\sqrt{2mE_{\text{kin}}}$, where $E_{\text{kin}} = h\nu - W - E_B$ and W is the work function, making the model $h\nu$ dependent.

Since atomic sites are positioned such that \mathcal{M}_y is broken, this will lead to different \mathbf{r}_j -derived phase shifts in $\langle e^{i\mathbf{k}_{fS1} \cdot \mathbf{r}} | \psi_i(\mathbf{k}_{iS1}, \mathbf{r}) \rangle$ and $\langle e^{i\mathbf{k}_{fS3} \cdot \mathbf{r}} | \psi_i(\mathbf{k}_{iS3}, \mathbf{r}) \rangle$. One can show that in a generic case this leads to different spin polarizations for the two emission directions \mathbf{k}_{fS1} and \mathbf{k}_{fS3} , despite equal initial state polarizations $S_{iy}(\mathbf{k}_{fS1})$ and $S_{iy}(\mathbf{k}_{fS3})$, as discussed earlier. A full derivation of this interference model for the minimal case of two orbitals on two different sites, which is lengthy but elementary, is presented in Sec. SIV of the Supplemental Material [26], while the complex orbital structure [Fig. 2(d)] forbids writing a realistic TB model of WTe_2 . The existence of the asymmetry for s -polarized light (Supplemental Material Fig. S4 [26]) is in agreement with both the interference model and one-step model calculations and points out that the effect is not related to breaking of the \mathcal{M}_x mirror plane by p -polarized light.

Figures 3(i)–3(m) illustrate sensitive dependence of the SARPES spin texture on various parameters. Importantly, the predicted effect at the experimental parameters (p -polarized light, $h\nu = 6 \text{ eV}$, light incidence angle 70°) is small, which calls for further improvement of the theoretical description that is critical in establishing whether WTe_2 realizes a Weyl type-II phase. These improvements can include further exploring correlation effects [15] and structural changes [16,36] and relaxations, which can lead to significant renormalization of the electronic structure and orbital character of the surface states.

Discussion.—Following the above arguments, we propose that establishing initial state spin textures experimentally shall involve iterative optimization of the agreement to the initial state and one-step model calculations, exploring the parameter space such as in Figs. 3(i)–3(m). Experimentally this is currently challenging, but might be feasible using the new generation spin detectors [29,37].

Furthermore, we propose that spin asymmetries as observed here shall be present in SARPES from every surface that exhibits spin-momentum locked bands and lacks the mirror plane perpendicular to one of the lateral directions. Similar effects have been studied theoretically, but not directly discussed, for topological insulators [35] and Rashba systems [38]. Regarding recent experimental work, the conventional analysis of SARPES spectra from 1T-HfSe₂ [39] could be augmented by considering the spin filtering effects in all the cases where incomplete spin reversal is observed between $\pm\mathbf{k}$ momenta that are not connected by the mirror plane.

The presented effect is different from the interference photoemission models for the generic orientation of the light polarization [40], since these models do not take into account phase shifts in the matrix element due to different locations of atomic sites. Spin filtering in photoemission through ultrathin ferromagnetic layers has been discussed previously [41], however, the effect in WTe₂ is different, since it does not involve time-reversal symmetry breaking in the initial state. Conversely, a filtering due to non-magnetic overlayers on magnetic substrates has also been studied [42], which is again different from the effect discussed here, since it involves a modification of the initial band structure.

Summary.—Low crystal symmetry of WTe₂, which is responsible for its exotic transport properties, leads to emerging asymmetries in the SARPES spin textures. We have characterized spin textures in the photoelectron ensemble from WTe₂ surfaces excited by the 6 eV continuous wave laser light. Despite the overall high asymmetry, the spin textures of adjacent terraces are connected by the \mathcal{M}_y mirror symmetry operation. Results have been obtained using a novel SARPES machine that enables 2D mapping of the spin textures with reduced instrumental asymmetries. The modulation of the photoelectron spin polarization can be interpreted as the geometry-induced, light-polarization-independent spin filtering effect, which can be modeled qualitatively within the free-electron final state photoemission model with the $\langle e^{i\mathbf{k}_f \cdot \mathbf{r}} | \psi(\mathbf{k}, \mathbf{r}) \rangle$ matrix element.

The surface spin texture of WTe₂ imaged over the extended momentum range illustrates a nontrivial connection between the initial state band structure properties and the photoelectron constant energy reciprocal space maps. Similar effects are expected in other quantum materials where a corresponding experimental geometry can be established. Generally, a more complete picture of electronic properties could be obtained by combining circular-dichroic and spin texture ARPES maps [43], which could address the orbital character of the participating states toward the identification of the transport-relevant Berry curvature hot spots [44]. In this way, our results call for future research to establish a connection between SARPES maps and initial state spin textures.

The authors would like to thank F. Freimuth, D. Nabok, S. Ghosh, J. Henk, and Ph. Rüßmann for fruitful discussions. Moreover, L. P. and T. H. acknowledge the support of Peter Baltzer (MB Scientific), Nicola Gatti (LEOS Solutions), and Matthias Escher (Focus GmbH). At different stages of this project, the position of T. H. was funded by the Deutsche Forschungsgemeinschaft (DFG, German Research Foundation) under Germany's Excellence Strategy—Cluster of Excellence Matter and Light for Quantum Computing (ML4Q) EXC 2004/1—390534769 and by the DFG Priority Program SPP1666. J. M. and J. S. would like to thank the CEDAMNF (Grant No. CZ.02.1.01/0.0/0.0/15_003/0000358) cofunded by the Ministry of Education, Youth and Sports of Czech Republic, and the GACR Project No. 20-18725S for funding. J. S. and F. R. acknowledge financial support from the DFG through the Würzburg-Dresden Cluster of Excellence on Complexity and Topology in Quantum Matter—*ct.qmat* (EXC 2147, Project ID 390858490). G. B. gratefully acknowledges the computing time granted through JARA-HPC on the supercomputer JURECA at Forschungszentrum Jülich.

*l.plucinski@fz-juelich.de

- [1] M. N. Ali, J. Xiong, S. Flynn, J. Tao, Q. D. Gibson, L. M. Schoop, T. Liang, N. Haldolaarachchige, M. Hirschberger, N. P. Ong, and R. J. Cava, Large, non-saturating magnetoresistance in WTe₂, *Nature (London)* **514**, 205 (2014).
- [2] A. A. Soluyanov, D. Gresch, Z. Wang, Q. Wu, M. Troyer, X. Dai, and B. A. Bernevig, Type-II Weyl semimetals, *Nature (London)* **527**, 495 (2015).
- [3] P. Rüßmann, A. P. Weber, F. Glott, N. Xu, M. Fanciulli, S. Muff, A. Magrez, P. Bugnon, H. Berger, M. Bode, J. H. Dil, S. Blügel, P. Mavropoulos, and P. Sessi, Universal scattering response across the type-II Weyl semimetal phase diagram, *Phys. Rev. B* **97**, 075106 (2018).
- [4] F. Y. Bruno, A. Tamai, Q. S. Wu, I. Cucchi, C. Barreateau, A. de la Torre, S. McKeown Walker, S. Riccò, Z. Wang, T. K. Kim, M. Hoesch, M. Shi, N. C. Plumb, E. Giannini, A. A. Soluyanov, and F. Baumberger, Observation of large topologically trivial Fermi arcs in the candidate type-II Weyl semimetal WTe₂, *Phys. Rev. B* **94**, 121112(R) (2016).
- [5] S. Tang *et al.*, Quantum spin hall state in monolayer 1T-WTe₂, *Nat. Phys.* **13**, 683 (2017).
- [6] V. Fatemi, S. Wu, Y. Cao, L. Bretheau, Q. D. Gibson, K. Watanabe, T. Taniguchi, R. J. Cava, and P. Jarillo-Herrero, Electrically tunable low-density superconductivity in a monolayer topological insulator, *Science* **362**, 926 (2018).
- [7] E. Sajadi, T. Palomaki, Z. Fei, W. Zhao, P. Bement, C. Olsen, S. Luescher, X. Xu, J. A. Folk, and D. H. Cobden, Gate-induced superconductivity in a monolayer topological insulator, *Science* **362**, 922 (2018).
- [8] I. Sodemann and L. Fu, Quantum Nonlinear Hall Effect Induced by Berry Curvature Dipole in Time-Reversal Invariant Materials, *Phys. Rev. Lett.* **115**, 216806 (2015).
- [9] Q. Ma, S.-Y. Xu, H. Shen, D. MacNeill, V. Fatemi, T.-R. Chang, A. M. M. Valdivia, S. Wu, Z. Du, C.-H. Hsu,

- S. Fang, Q. D. Gibson, K. Watanabe, T. Taniguchi, R. J. Cava, E. Kaxiras, H.-Z. Lu, H. Lin, L. Fu, N. Gedik, and P. Jarillo-Herrero, Observation of the nonlinear Hall effect under time-reversal-symmetric conditions, *Nature (London)* **565**, 337 (2019).
- [10] K. Kang, T. Li, E. Sohn, J. Shan, and K. F. Mak, Nonlinear anomalous hall effect in few-layer WTe₂, *Nat. Mater.* **18**, 324 (2019).
- [11] Z. Z. Du, H.-Z. Lu, and X. C. Xie, Nonlinear Hall effects, *Nat. Rev. Phys.* **3**, 744 (2021).
- [12] I. Pletikosić, M. N. Ali, A. V. Fedorov, R. J. Cava, and T. Valla, Electronic Structure Basis for the Extraordinary Magnetoresistance in WTe₂, *Phys. Rev. Lett.* **113**, 216601 (2014).
- [13] Y. Wu, N. H. Jo, M. Ochi, L. Huang, D. Mou, S. L. Bud'ko, P. C. Canfield, N. Trivedi, R. Arita, and A. Kaminski, Temperature-Induced Lifshitz Transition in WTe₂, *Phys. Rev. Lett.* **115**, 166602 (2015).
- [14] C.-L. Wang *et al.*, Evidence of electron-hole imbalance in WTe₂ from high-resolution angle-resolved photoemission spectroscopy, *Chin. Phys. Lett.* **34**, 097305 (2017).
- [15] D. Di Sante, P. K. Das, C. Bigi, Z. Ergönenc, N. Gürtler, J. A. Krieger, T. Schmitt, M. N. Ali, G. Rossi, R. Thomale, C. Franchini, S. Picozzi, J. Fujii, V. N. Strocov, G. Sangiovanni, I. Vobornik, R. J. Cava, and G. Panaccione, Three-Dimensional Electronic Structure of the Type-II Weyl Semimetal WTe₂, *Phys. Rev. Lett.* **119**, 026403 (2017).
- [16] A. Rossi, G. Resta, S. H. Lee, R. D. Redwing, C. Jozwiak, A. Bostwick, E. Rotenberg, S. Y. Savrasov, and I. M. Vishik, Two phase transitions driven by surface electron doping in WTe₂, *Phys. Rev. B* **102**, 121110(R) (2020).
- [17] B. Feng, Y.-H. Chan, Y. Feng, R.-Y. Liu, M.-Y. Chou, K. Kuroda, K. Yaji, A. Harasawa, P. Moras, A. Barinov, W. Malaeb, C. Bareille, T. Kondo, S. Shin, F. Komori, T.-C. Chiang, Y. Shi, and I. Matsuda, Spin texture in type-II Weyl semimetal WTe₂, *Phys. Rev. B* **94**, 195134 (2016).
- [18] M. Fanciulli, J. Schusser, Min-I. Lee, Z. E. Youbi, O. Heckmann, M. C. Richter, C. Cacho, C. Spezzani, D. Bresteau, J. F. Hergott, P. D'Oliveira, O. Tcherbakoff, T. Ruchon, J. Minár, and K. Hricovini, Spin, time, and angle resolved photoemission spectroscopy on WTe₂, *Phys. Rev. Res.* **2**, 013261 (2020).
- [19] Y. Wan, L. Wang, K. Kuroda, P. Zhang, K. Koshiishi, M. Suzuki, J. Kim, R. Noguchi, C. Bareille, K. Yaji, A. Harasawa, S. Shin, S.-W. Cheong, A. Fujimori, and T. Kondo, Selective observation of surface and bulk bands in polar WTe₂ by laser-based spin- and angle-resolved photoemission spectroscopy, *Phys. Rev. B* **105**, 085421 (2022).
- [20] M. Escher, N. B. Weber, M. Merkel, L. Plucinski, and C. M. Schneider, Ferrum: A new highly efficient spin detector for electron spectroscopy, *e-J. Surf. Sci. Nanotechnol.* **9**, 340 (2011).
- [21] T. Okuda, Y. Takeichi, Y. Maeda, A. Harasawa, I. Matsuda, T. Kinoshita, and A. Kakizaki, A new spin-polarized photoemission spectrometer with very high efficiency and energy resolution, *Rev. Sci. Instrum.* **79**, 123117 (2008).
- [22] C. Bigi, P. K. Das, D. Benedetti, F. Salvador, D. Krizmancic, R. Sergo, A. Martin, G. Panaccione, G. Rossi, J. Fujii, and I. Vobornik, Very efficient spin polarization analysis (VESPA): New exchange scattering-based setup for spin-resolved ARPES at APE-NFFA beamline at Elettra, *J. Synchrotron Radiat.* **24**, 750 (2017).
- [23] J. P. Perdew, K. Burke, and M. Ernzerhof, Generalized Gradient Approximation Made Simple, *Phys. Rev. Lett.* **77**, 3865 (1996).
- [24] FLEUR, <https://www.flapw.de>.
- [25] J. Braun, J. Minár, and H. Ebert, Correlation, temperature and disorder: Recent developments in the one-step description of angle-resolved photoemission, *Phys. Rep.* **740**, 1 (2018).
- [26] See Supplemental Material at <http://link.aps.org/supplemental/10.1103/PhysRevLett.130.146401> for the details of experimental and theoretical methods, which includes Refs. [14–16, 18, 20–25, 27–32].
- [27] A. Mar, S. Jobic, and J. A. Ibers, Metal-metal vs tellurium-tellurium bonding in WTe₂ and its ternary variants TaIrTe₄ and NbIrTe₄, *J. Am. Chem. Soc.* **114**, 8963 (1992).
- [28] C. Li, A. J. Freeman, H. J. F. Jansen, and C. L. Fu, Magnetic anisotropy in low-dimensional ferromagnetic systems: Fe monolayers on Ag(001), Au(001), and Pd(001) substrates, *Phys. Rev. B* **42**, 5433 (1990).
- [29] C. Tusche, A. Krasnyuk, and J. Kirschner, Spin resolved bandstructure imaging with a high resolution momentum microscope, *Ultramicroscopy* **159**, 520 (2015).
- [30] E. Tamura and R. Feder, Spin polarization in normal photoemission by linearly polarized light from nonmagnetic (001) surfaces, *Europhys. Lett.* **16**, 695 (1991).
- [31] J. Henk, T. Scheunemann, and R. Feder, Spin polarization in valence-band photoemission from non-magnetic (001) surfaces, *J. Phys. Condens. Matter* **9**, 2963 (1997).
- [32] Y. Wu, N. H. Jo, D. Mou, L. Huang, S. L. Bud'ko, P. C. Canfield, and A. Kaminski, Three-dimensionality of the bulk electronic structure in WTe₂, *Phys. Rev. B* **95**, 195138 (2017).
- [33] A. P. Weber, P. Rüßmann, N. Xu, S. Muff, M. Fanciulli, A. Magrez, P. Bugnon, H. Berger, N. C. Plumb, M. Shi, S. Blügel, P. Mavropoulos, and J. H. Dil, Spin-Resolved Electronic Response to the Phase Transition in MoTe₂, *Phys. Rev. Lett.* **121**, 156401 (2018).
- [34] S. Moser, An experimentalist's guide to the matrix element in angle resolved photoemission, *J. Electron Spectrosc. Relat. Phenom.* **214**, 29 (2017).
- [35] Z.-H. Zhu, C. N. Veenstra, G. Levy, A. Ubaldini, P. Syers, N. P. Butch, J. Paglione, M. W. Haverkort, I. S. Elfimov, and A. Damascelli, Layer-by-Layer Entangled Spin-Orbital Texture of the Topological Surface State in Bi₂Se₃, *Phys. Rev. Lett.* **110**, 216401 (2013).
- [36] J. Xiao, Y. Wang, H. Wang, C. D. Pemmaraju, S. Wang, P. Muscher, E. J. Sie, C. M. Nyby, T. P. Devereaux, X. Qian, X. Zhang, and A. M. Lindenberg, Berry curvature memory through electrically driven stacking transitions, *Nat. Phys.* **16**, 1028 (2020).
- [37] G. Schönhense, K. Medjanik, and H.-J. Elmers, Space-, time- and spin-resolved photoemission, *J. Electron Spectrosc. Relat. Phenom.* **200**, 94 (2015).
- [38] H. Bentmann, H. Maaß, E. E. Krasovskii, T. R. F. Peixoto, C. Seibel, M. Leandersson, T. Balasubramanian, and F. Reinert, Strong Linear Dichroism in Spin-Polarized Photoemission from Spin-Orbit-Coupled Surface States, *Phys. Rev. Lett.* **119**, 106401 (2017).

- [39] O. J. Clark, O. Dowinton, M. S. Bahramy, and J. Sánchez-Barriga, Hidden spin-orbital texture at the $\bar{\Gamma}$ -located valence band maximum of a transition metal dichalcogenide semiconductor, *Nat. Commun.* **13**, 4147 (2022).
- [40] K. Yaji, K. Kuroda, S. Toyohisa, A. Harasawa, Y. Ishida, S. Watanabe, C. Chen, K. Kobayashi, F. Komori, and S. Shin, Spin-dependent quantum interference in photoemission process from spin-orbit coupled states, *Nat. Commun.* **8**, 14588 (2017).
- [41] J. Henk, P. Bose, T. Michael, and P. Bruno, Spin motion of photoelectrons, *Phys. Rev. B* **68**, 052403 (2003).
- [42] T. Berdot, A. Hallal, L. T. Bismaths, L. Joly, P. Dey, J. Henk, M. Alouani, and W. Weber, Effect of submonolayer MgO coverages on the electron-spin motion in Fe(001): Experiment and theory, *Phys. Rev. B* **82**, 172407 (2010).
- [43] H. Mirhosseini and J. Henk, Spin Texture and Circular Dichroism in Photoelectron Spectroscopy from the Topological Insulator Bi_2Te_3 : First-Principles Photoemission Calculations, *Phys. Rev. Lett.* **109**, 036803 (2012).
- [44] M. Schüler, T. Pincelli, S. Dong, T. P. Devereaux, M. Wolf, L. Rettig, R. Ernstorfer, and S. Beaulieu, Polarization-Modulated Angle-Resolved Photoemission Spectroscopy: Toward Circular Dichroism without Circular Photons and Bloch Wave-Function Reconstruction, *Phys. Rev. X* **12**, 011019 (2022).